OPEN

NPG Asia Materials (2016) 8, e303; doi:10.1038/am.2016.108
www.nature.com/am

ORIGINAL ARTICLE

Approaching ultimate flexible organic light-emitting diodes using a graphene anode

Tae-Hee Han[1,3], Min-Ho Park[1,3], Sung-Joo Kwon[1], Sang-Hoon Bae[2], Hong-Kyu Seo[1], Himchan Cho[1], Jong-Hyun Ahn[2] and Tae-Woo Lee[1]

Ultimate flexible organic light-emitting diodes (OLEDs) should have an ultra-high device efficiency, a low-efficiency roll-off at a high luminance and excellent flexibility. Here, we realized flexible tandem OLEDs using a graphene anode with a very high electroluminescent efficiency of ~205.9 cd A^{-1}, 45.2% (~396.4 cd A^{-1}, 87.3% with a hemispherical lens) and a very low efficiency roll-off at a high luminance of ~6.6% at 10 000 cd m^{-2} (~3.8% with a hemispherical lens) by stacking two organic electroluminescence (EL) units. For the first time, we used an easily controlled and low-temperature processable charge generation layer with lithium nitride (Li_3N). This simultaneously provided efficient stacking of EL units and enhanced compatibility of the flexible device on a thin plastic substrate. The flexible tandem OLEDs with a graphene anode also showed great flexibility against bending up to a bending strain of 6.7%. These results represent a significant advancement towards the production of next-generation flexible displays and solid-state lighting that use a graphene anode.
NPG Asia Materials (2016) **8,** e303; doi:10.1038/am.2016.108; published online 9 September 2016

INTRODUCTION

Organic light-emitting diodes (OLEDs) have shown a strong potential for use in next-generation flexible displays and solid-state lighting.[1–8] However, indium–tin oxide (ITO), the most widely used electrode in OLEDs, has a very poor tolerance to external mechanical stress.[9] Furthermore, its cost has increased gradually owing to a scarcity of indium.[9] In and Sn ions that diffuse from the ITO electrode to overlying layers can act as charge-trapping centers during the charge injection process, and this degrades the luminous efficiency and operational stability of organic opto-electronic devices owing to the exciton quenching effect of In and Sn atomic species.[6,9] Therefore, ITO-based electronic devices are unsuitable for practical flexible electronics. To enable the fabrication of flexible organic opto-electronic devices, the brittle ITO electrode should be replaced with a flexible transparent conducting electrode. Much effort has been made to replace the ITO electrode with transparent conducting materials such as conducting polymers, carbon nanotubes and metal nanowires.[10–12] Among these materials, graphene, which is a two-dimensional sheet of sp^2-bonded carbon atoms, provides several advantages for flexible transparent electrodes, such as high optical transparency, low sheet resistance, excellent flexibility, smooth surface (thus preventing electrical shortage in devices), and no optical haze.[13–19] The chemical stability of graphene is an additional advantage for its practical use in organic opto-electronic devices.[6,16,17] Therefore, several researchers have considered the possibility of using graphene electrodes in flexible organic opto-electronics.[6,20–31] There has been significant progress in the use of flexible OLEDs with graphene electrodes because of the existence of methods to modify the high sheet resistance ($>300\ \Omega$ per square) and low work function (WF) (~4.4 eV) of pristine graphene.[6,20–27,32,33] However, in recently reported OLEDs with graphene anodes, further improvements are needed in areas such as the electroluminescent efficiency, the efficiency roll-off at a high luminance and the experimental verification of device flexibility to achieve ideal flexible OLEDs. To enable further advances towards the ultimate goal of flexible OLEDs for practical use, several requirements must be met at the same time: (i) ultra-high efficiency over that of state-of-the-art OLEDs that use a rigid electrode and substrate, (ii) very low reduction in device efficiency at high luminance (i.e., efficiency roll-off) and (iii) excellent flexibility. For a successful switch from rigid to flexible electronics, it is important to realize ultra-high efficiency in flexible OLEDs without sacrificing the device efficiency of state-of-the-art rigid OLEDs. Additionally, the large device efficiency roll-off of OLEDs should be minimized for practical use at high luminance. Here, to meet all these requirements, we fabricated tandem OLEDs by stacking two electroluminescence (EL) units vertically on a modified graphene anode to increase the luminous current efficiency (CE) and external quantum efficiency (EQE) and to reduce the efficiency roll-off at high luminance (Figures 1a and b). Fabricating tandem OLEDs by stacking two EL units is a very effective way to reduce the current density at the

[1]Department of Materials Science and Engineering, Pohang University of Science and Technology (POSTECH), Gyungbuk, Republic of Korea and [2]School of Electrical & Electronic Engineering, Yonsei University, Seoul, Republic of Korea
[3]These authors contributed equally to this work.
Correspondence: Professor T-W Lee, Department of Materials Science and Engineering, Pohang University of Science and Technology (POSTECH), 77 Cheongam-Ro, Nam-Gu, Pohang, Gyungbuk 790-784, Republic of Korea.
E-mail: twlee@postech.ac.kr or taewlees@gmail.com
Received 15 April 2016; revised 1 June 2016; accepted 11 June 2016

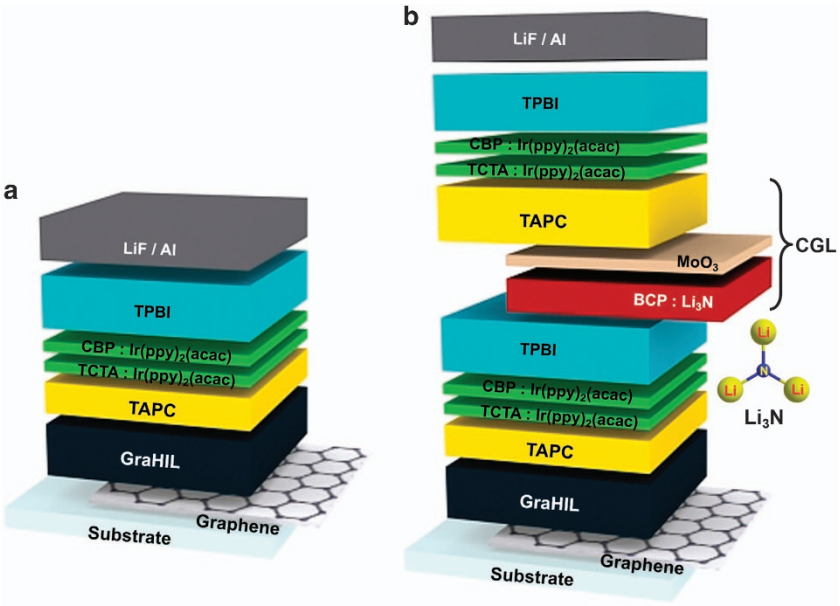

Figure 1 Device architectures of (**a**) standard single-unit OLEDs and (**b**) tandem OLEDs including two EL units and charge generation layer using Li_3N.

same luminance, and it can significantly increase CE and EQE and simultaneously reduce the efficiency roll-off at high luminance.[34,35] However, in-line mass production of highly flexible tandem OLEDs on thin plastic substrates with low thermal resistance will be difficult when the substrates are exposed to high temperatures above the glass transition temperature for a long time. Therefore, it is important to avoid high temperature evaporation processes as much as possible during the in-line production process. With this in mind, we developed and used a low-temperature-processable charge generation layer (CGL) between two EL units that is formed by a stable co-deposition of the organic electron transporting layer (ETL) and an n-type metal dopant in a single organic chamber. The CGL can effectively generate and inject charge carriers with enhanced compatibility for flexible devices on a thin plastic substrate. Finally, we achieved very flexible tandem OLEDs with a graphene anode on a thin plastic substrate.

MATERIALS AND METHODS

Fabrication and characterization of the graphene anode

Rollable Cu foils were used in quartz tubes of a chemical vapor deposition (CVD) system for growing large-area single layer graphene (SLG). Cu foils in the CVD chamber were heated to 1040 °C for 30 min and then annealed for 30 min at 1040 °C with a 15 sccm H_2 gas flow (pressure ~ 150 mTorr). During the graphene growth, precursor CH_4 was injected at a flow rate of 60 sccm for 30 min (pressure ~ 700 mTorr). After the growth step, the Cu foils were cooled rapidly to room temperature. Poly(methyl methacrylate) ((molecular weight: 996 000 g mol^{-1}) purchased from Sigma Aldrich (St Louis, MO, USA), 4.6 g in 100 ml chlorobenzene) was spin-coated on the graphene on top of the Cu foils to make a supporting polymer layer. The Cu foils were then etched using CE-100 etchant for 1 h and rinsed with deionized water to remove residual etchant. To fabricate multi-layered graphene films, the graphene/polymer support layer was transferred to the poly(ethylene terephthalate) (PET) or glass substrate, and then the poly(methyl methacrylate)-supporting layer was removed by immersion in acetone for 30 min. This step was performed repeatedly to stack SLGs on the target substrates. The four-layered graphenes (4LGs) were p-type-doped by exposure to HNO_3 vapor for 150 s, and successively dried in vacuum (~10^{-3} Torr) for 20 min to remove excess HNO_3 molecules on the graphene anode. The HNO_3 vapor doping reduced the sheet resistance of the 4LG on a PET substrate to $58.3 \pm 3.8\ \Omega$ per square. Although the sheet resistance of the graphene used in this work is relatively low, it is necessary to further improve the electrical conductivity and create a smoother surface morphology of the graphene for large-area applications and long-term operation. Therefore, (i) understanding the growth mechanism for graphene with large size domains and well-connected grain boundaries, (ii) developing a transfer process for defect-free and residue-free graphene films, and (iii) developing an efficient p-type doping method are still important research topics.

Optical transmittance was measured using a SCINCO S-3100 (Seoul, Korea) and Raman spectroscopy was performed using a WITEC (Ulm, Germany) with a 532-nm laser to confirm the success of graphene growth and transfer.

Fabrication and characterization of OLEDs

The graphene anodes on glass or PET substrates were ultra-violet ozone treated for 10 min. Then, 50–60 nm thick GraHIL (a polymer blend of Poly(3,4-ethylenedioxythiophene)-poly(styrenesulfonate) (PEDOT:PSS) (CLEVIOS P VP AI4083) and a tetra-fluoroethylene-perfluoro-3,6-dioxa-4-methyl-7-octenesulfonic acid copolymer (PFI), CAS number: 31175-20-9, with a weight ratio of 1:3.6) was spin-coated on the ultra-violet ozone treated anodes and baked on a hot plate in air at 150 °C for 30 min. The other OLED layers were sequentially deposited on the GraHIL in a thermal vacuum evaporator under 5×10^{-7} Torr. Di-[4-(*N*,*N*-ditolyl-amino)-phenyl]cyclohexane (TAPC) (15 nm) and (1,3,5-tri (phenyl-2-benzimidazolyl)-benzene (TPBI) (55 nm) were used as the hole transporting layer (HTL) and ETL, respectively. To deposit the emitting layer, host materials and phosphorescent dopant materials were co-evaporated (97:3 (v/v) 1,1-bis[4-[*N*,*N*-di(*p*-tolyl)amino]phenyl]cyclohexane (TCTA):bis(2-phenylpyridine) iridium (III) acetylacetonate (Ir(ppy)2(acac)) and 96:4 (v/v) 4,4′-*N*,*N*′-dicarbazolylbiphenyl (CBP):$Ir(ppy)_2(acac)$). To form a CGL between two EL units, 2,9-dimethyl-4,7-diphenyl-1,10-phenanthroline (BCP) and lithium nitride (Li_3N) (>99.5%, CAS number: 26134-62-3; Sigma-Aldrich) (9:1 (v/v)) were co-evaporated as an n-type-doped layer. Then, 5-nm-thick molybdenum trioxide (MoO_3) and 65-nm-thick TAPC were sequentially deposited for charge generation and injection. A cathode layer (lithium fluoride (LiF) (1 nm)/Al (130 nm)) was deposited at the end of the evaporation process. Current–voltage–luminance characterization was performed using a Keithley 236 power source from Keithley Instruments (Cleveland, OH, USA) and a Minolta CS-2000 EL spectroradiometer from Konica Minolta (Tokyo, Japan). To measure enhancement of light output with a hemispherical lens, a 6-inch integrating sphere (IS-6; StellarNet, Tampa, FL, USA) and a calibrated BLUE-Wave spectrometer (BW-VIS; StellarNet) (range: 400–1100 nm) were used. The hemispherical lens is a half-ball type lens (radius: 5 mm, thickness: 5 mm;

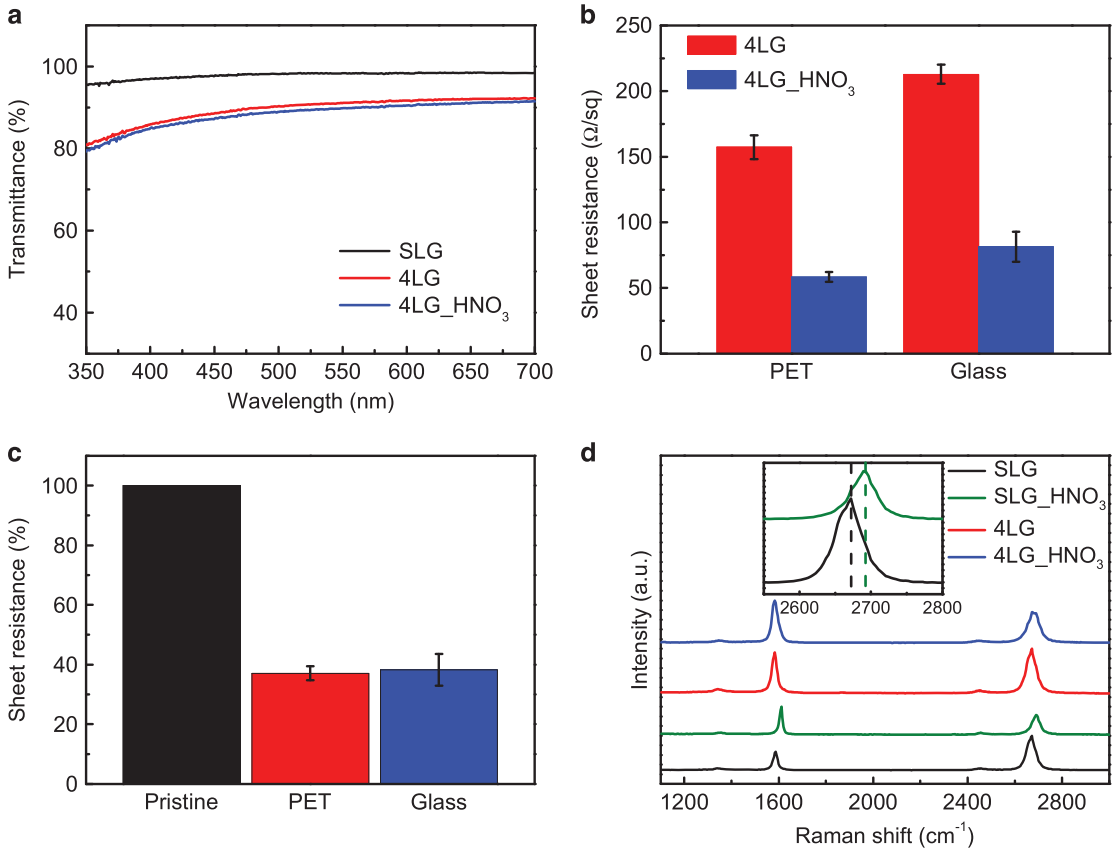

Figure 2 (**a**) UV–vis optical transmittance of SLG, 4LG and HNO_3-doped 4LG. (**b**) Sheet resistance of 4LGs. (**c**) Change of sheet resistance according to substrate. (**d**) Raman spectra of pristine SLG, HNO_3-doped SLG, pristine 4LG, and HNO_3-doped 4LG.

Admund Optics, Barrington, NJ, USA). Index matching fluid (F-IMF-105; Newport, Santa Clara, CA, USA) (refractive index: 1.52 at 589 nm, viscosity: 100 cps) was used between the device substrate and the hemispherical lens.

RESULTS AND DISCUSSION

To obtain high-quality graphene sheets, we employed CVD using Cu catalyst foils to synthesize large sheets of SLG (Supplementary Table S1). The SLG on Cu foils was repeatedly transferred onto a PET or glass substrates using a poly(methyl methacrylate) support. The transferred SLG on a glass substrate exhibited high optical transparency (~98%), and 4LG films, formed by stacking SLGs, showed >91% optical transparency at 550 nm (Figure 2a). The optical transparency decreased by ~2.3% per layer of stacked SLGs; this gradual decrease ensures that stacking of SLGs for the multi-layered graphene anode does not disrupt the optical properties of the SLGs. The 4LG films were chemically p-doped using HNO_3 vapor to reduce the high sheet resistance of the pristine 4LG anode on a PET substrate from $157.2 \pm 9.1\ \Omega$ per square (pristine) to $58.3 \pm 3.8\ \Omega$ per square (HNO_3-doped) (Figure 2b, Supplementary Table S2). The 4LG transferred onto a glass substrate had a higher sheet resistance (pristine: $212.7 \pm 7.2\ \Omega$ per square and HNO_3-doped: $81.3 \pm 11.3\ \Omega$ per square) than those on PET. The difference can be attributed to the lower adhesion energy of pristine graphene with glass substrates than with polymer substrates; during transfer of SLG, the low adhesion energy between graphene and the substrate can induce defects in graphene sheets that decrease the electrical properties of the graphene.[36,37] HNO_3 p-type doping led to an ~62% decrease in the sheet resistance of pristine graphene on both PET and glass substrates (Figure 2c). Although the optical transparency decreased slightly when 4LG sheets were doped by HNO_3 vapor, the p-doped 4LG anode maintained a satisfactory optical transparency of ~90% (Figure 2a).

The SLG growth quality and graphene stacking were confirmed using Raman spectroscopy (Figure 2d). The intensity ratio of the 2D (~2672 cm^{-1}) to G (~1587 cm^{-1}) band of SLG was ~1.9, and that of the D (~1350 cm^{-1}) to G (~1587 cm^{-1}) band was negligible compared with the other characteristic bands of graphene in the Raman spectra; these results demonstrated that high-quality SLG was successfully grown and transferred onto the substrate. The stacking of SLG to form 4LG anode decreased the intensity ratio of the 2D to G band to ~1.1 and broadened the 2D band; this was caused by local interactions between SLGs.[38,39] Upshifts of the 2D (2672 to 2691 cm^{-1}) and G (1587 to 1611 cm^{-1}) bands and a decrease in the intensity ratio of the 2D to G band (Figure 2d) also indicated that an effective p-type doping of graphene was achieved using HNO_3 vapor.[18,38,39] All the Raman spectra shown in Figure 2d are averaged results of large-area ($50 \times 50\ \mu m^2$) mapping of graphene surfaces.

We also used a polymeric gradient hole injection layer (GraHIL) composed of PEDOT:PSS and PFI to facilitate hole injection from the graphene anode which has a low WF (~4.4 eV).[6] Because the HTL and emitting layer have much deeper highest occupied molecular orbital (HOMO) energy levels (e.g., TAPC ~5.4 eV) than the WF of pristine graphene, the pristine graphene film forms a large hole injection energy barrier, >1.0 eV.[40] The GraHIL gives the graphene anode a high surface WF (~5.95 eV) and efficient hole injection

Table 1 CE, EQE and efficiency roll-off of single and tandem OLEDs with a graphene anode

Device	Max. CE ($cd\ A^{-1}$)	Max. EQE (%)	CE (10 000 $cd\ m^{-2}$) ($cd\ A^{-1}$)	EQE (10 000 $cd\ m^{-2}$) (%)	Efficiency roll-off (10 000 $cd\ m^{-2}$) (%)
Single glass/graphene	120.8	32.7	91.1	22.8	32.6
Tandem PET/graphene	205.9	45.2	193.2	42.4	6.6
Tandem glass/graphene	202.9	44.4	181.7	39.7	11.7
Tandem PET/graphene (HS lens)	395.0	86.5	380.5	83.4	3.8
Tandem glass/graphene (HS lens)	396.4	87.3	364.4	80.2	8.8

by establishing a gradient ionization potential that is developed by self-organization; this gradient concentration of PFI is from the bottom-facing graphene anode to the top-facing HTL (Supplementary Table S3 and Supplementary Figures S1 and S2).[6]

Using 4LG films as the flexible transparent conducting anode, we fabricated standard OLEDs consisting of a single EL unit and tandem OLEDs stacked with two EL units (Figures 1a and b). To fabricate high-efficiency OLEDs, we used heteroleptic iridium complex ($Ir(ppy)_2(acac)$) as a green phosphorescent dopant that prefers horizontal dipole orientation; this can increase the optical light out-coupling of OLED devices.[41] As we increased the number of graphene layers by stacking SLGs on the substrate, the anode's electrical conductivity and work function increased gradually, but its optical transparency decreased simultaneously. Therefore, we chose the 4LG that provides the optimal number of graphene layers for flexible OLEDs by considering the trade-off between electrical properties and optical transparency.[6] Although green phosphorescent single-unit OLEDs with a 4LG showed high CE $\sim 120.8\ cd\ A^{-1}$ and EQE $\sim 32.7\%$ (Table 1 and Supplementary Figure S3), standard single-unit OLEDs suffered from large efficiency roll-off characteristics: $>30\%$ decrease of maximum CEs and EQEs at high luminance ($\sim 10\,000\ cd\ m^{-2}$) (Table 1, Supplementary Figure S3). This result can be attributed to the relatively low electrical conductivity of the 4LG anode because the relatively high sheet resistance of graphene can limit the anodic current at high voltages and the charge balance of electrons and holes in OLEDs can change slightly as the applied voltage increases. This indicates that in flexible OLEDs with a graphene anode, the required current density to emit high luminance should be decreased to minimize the reduction in efficiency at high luminance.

To achieve an efficient vertical stacking of two EL units, a CGL should be inserted between them. Alkali metal derivatives which include low WF alkali metals (e.g., Li, Cs, Mg) are generally used as n-type dopants in a CGL. These types of alkali metal derivatives (e.g., LiF, Cs_2CO_3) are generally evaporated at a much higher temperature than widely used organic materials in OLEDs. A co-deposition of high-temperature evaporable n-type dopants and typical low-temperature evaporable organic materials is difficult to control precisely owing to out-gassing of organic materials in the vacuum chamber during high-temperature heating. Furthermore, high-temperature heating of a device on the thin plastic PET substrate with low thermal resistance (glass transition temperature of PET: 78 °C) for a long time can result in damage to the device owing to excessive strain and deformation.[42,43] To reduce the thermal damage to the thin PET substrate and to generate charges effectively, low-temperature evaporable n-type dopants can be used when fabricating flexible tandem OLEDs. Therefore, we used Li_3N as the easily controllable n-type dopant that evaporates at a low temperature in the CGL. The Li_3N thermally decomposes to Li and N_2 at ~ 300 °C under 5×10^{-5} Pa, conditions that are comparable to those for general

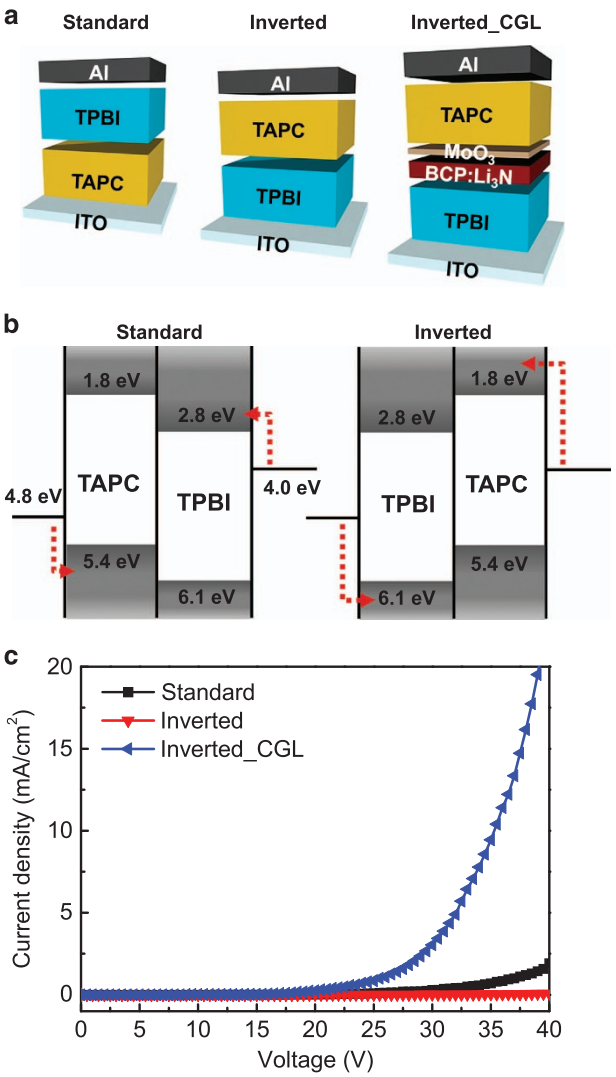

Figure 3 (**a**) Schematic drawings of three types of devices (standard, inverted and inverted structure with CGL). (**b**) Energy band diagrams of standard and inverted structured devices. (**c**) Current density versus applied forward bias in the three types of devices.

organic materials.[44] Only free Li atoms are deposited and contribute to n-type doping of organic materials; N_2 does not react with organic devices.[44] We believe that this type of approach, using low-temperature evaporable n-type dopants, would help to reduce high-temperature evaporation for practical applications; it overcomes the inherent difficulty of in-line mass production of flexible OLEDs on plastic substrates where substrates are exposed to high-temperature

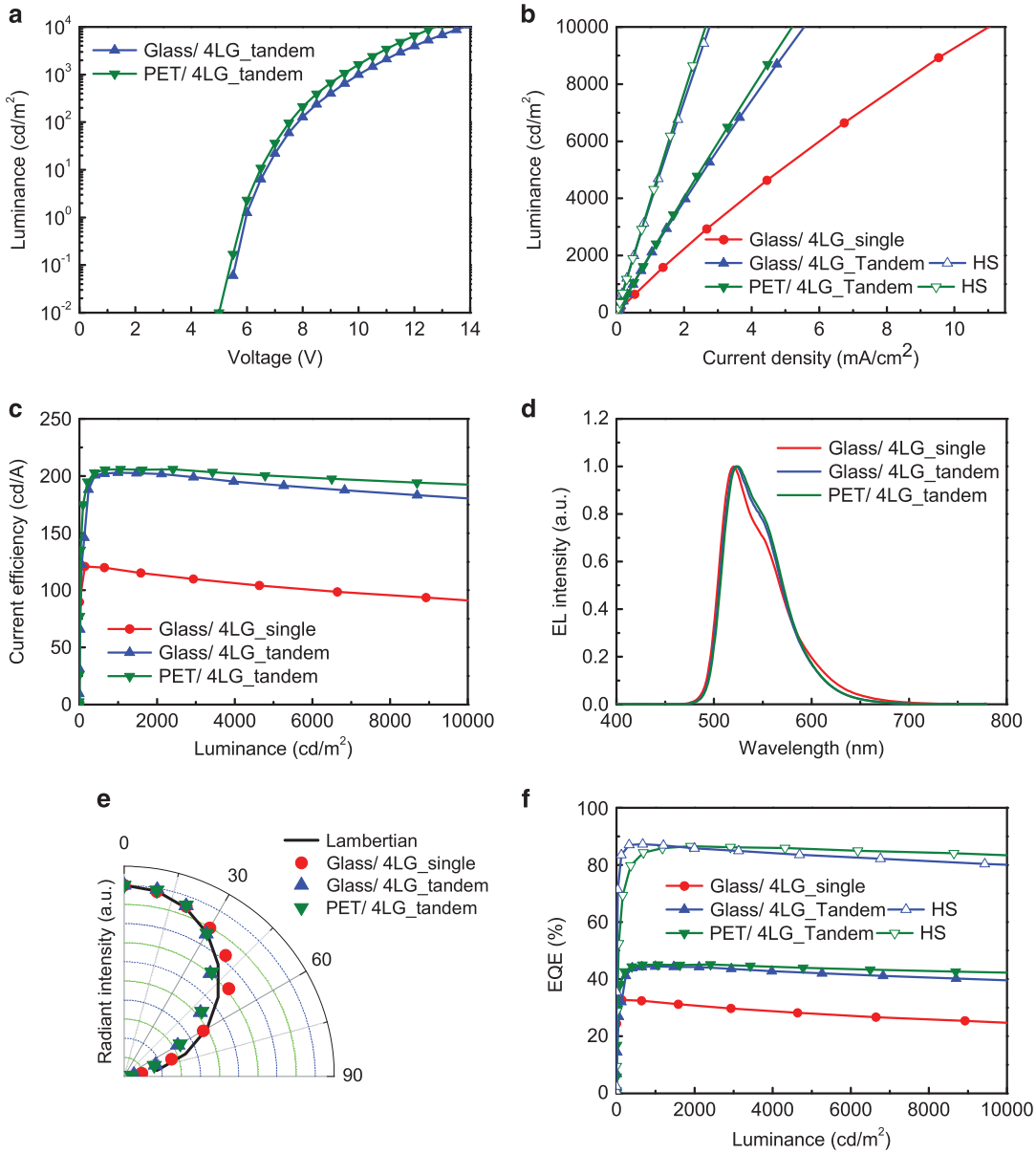

Figure 4 Luminance characteristics versus (**a**) applied voltage and (**b**) current density. (**c**) Current efficiencies versus luminance, (**d**) EL spectra and (**e**) angular EL distributions according to viewing angles of single-unit and tandem OLEDs with 4LG anode on a PET or a glass substrate. (**f**) Calculated external quantum efficiencies of single-unit, tandem OLEDs and tandem OLEDs with hemi-spherical (HS) lens using a graphene anode on a PET or a glass substrate.

heat for a long time during the manufacturing process. We employed a CGL composed of an organic electron-transporting material (BCP) doped with Li_3N, MoO_3, and a hole-transporting TAPC. To evaluate the ability of our CGL to generate charges, we performed charge spouting measurement by fabricating three types of devices (Figure 3a): (i) a standard device (ITO/HTL (TAPC) (300 nm)/ETL (TPBI) (250 nm)/Al); (ii) an inverted device (ITO/ETL (TPBI) (250 nm)/HTL (TAPC) (300 nm)/Al); and (iii) an inverted device with CGL (ITO/ETL (TPBI) (250 nm)/BCP: Li_3N (20 nm, 10%)/ MoO_3 (5 nm)/HTL (TAPC) (300 nm)/Al). By using this type of current–voltage measurement, we optimized the thickness of the n-doped organic ETL and the doping concentrations of Li_3N in CGL for efficient charge generation and injection (Supplementary Figure S4). The large energy barriers for hole (~0.6 eV) and electron (~1.2 eV) injection make it difficult for current to flow in the standard device. Under a positive applied bias, the inverted device has much less current flow than the standard device because the inverted device has larger charge injection energy barriers between the anode/ETL for holes (~1.3 eV) and cathode/HTL for electrons (~2.2 eV) than the standard device (Figure 3b). This result shows that stacking EL units without a CGL will obviously degrade the performance of OLEDs. In the CGL fabricated with a transition metal oxide, holes and electrons are generated at the interface between MoO_3 and HTL, and the applied positive bias injects charge carriers into the two EL units separately.[45,46] Because MoO_3 has a very deep-lying lowest unoccupied molecular orbital (LUMO) energy level (~6.0 eV), which is closely pinned to the Fermi energy level, generated holes can be easily injected into the HTL without a charge injection barrier (the HOMO of TAPC

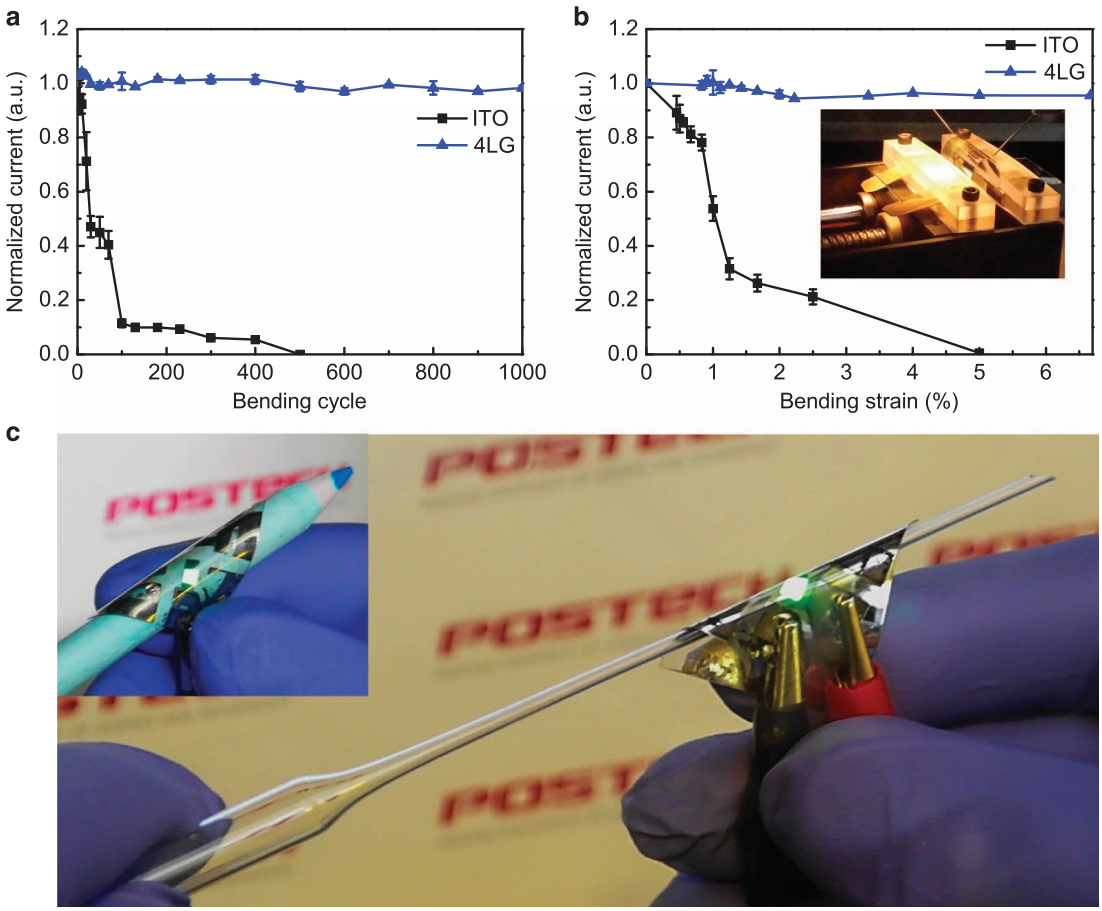

Figure 5 Normalized current density according to (**a**) bending cycles (bending radius of curvature: ~7.5 mm, bending strain: ~1.33%) and (**b**) bending strain (inset: optical image of flexible OLEDs with bending test machine). (**c**) Optical images of flexible OLEDs with a graphene anode wrapped on cylinders with different curvatures.

is ~5.4 eV). On the other hand, the highly n-type-doped organic layer and MoO_3 form a large interface dipole, and thus the vacuum level shifts at the interface between the BCP:Li_3N and MoO_3. This vacuum level shift at the interface facilitates electron injection from the MoO_3 layer into the ETL with a very narrow electron tunnelling barrier.[45,46] As a result, the insertion of this CGL between ETL and HTL in the inverted device provides a substantial increase in the current density of the device (Figure 3c); this means that the CGL can efficiently generate charge carriers and that the generated electrons and holes can be easily spouted into two EL units separately under positive applied bias.

By inserting our CGL between two EL units, we fabricated flexible green phosphorescent tandem OLEDs with 4LG on PET and glass substrates (Figure 1b). The tandem OLEDs with a 4LG anode on a PET substrate had better luminescent characteristics than the OLEDs on the glass substrate at a given applied voltage owing to the lower sheet resistance of the 4LG transferred onto the PET substrate (~$58.3 \pm 3.8\,\Omega$ per square) than that transferred onto the glass substrate (~$81.3 \pm 11.4\,\Omega$ per square) (Figures 2b and 4a). Tandem OLEDs with the graphene anode showed superior luminescent characteristics at the same current density compared with single-unit OLEDs (Figure 4b). Because the CGL generates and separately injects opposite charges into the upper and lower EL units under an applied forward bias, both EL units in the tandem OLED emit light at the same time. Therefore, tandem OLEDs require much less current density than single-unit OLEDs to emit a same luminance. In our device results, tandem OLEDs with the 4LG anode exhibited a high luminance (~10 000 cd m^{-2}) at a low current density (~5.2 mA cm^{-2} (PET) and 5.5 mA cm^{-2} (glass)), whereas a conventional single-unit OLED with the 4LG anode required over double the current density (~11 mA cm^{-2}) (Figure 4b). Tandem OLEDs with the 4LG anode exhibited very high CEs (~205.9 cd A^{-1} (PET) and 202.9 cd A^{-1} (glass)) with a low efficiency roll-off (Figure 4c). The single-unit OLED with the 4LG anode on glass showed a CE of ~91.9 cd A^{-1} at ~10 000 cd m^{-2} that decreased by 32.6% of its maximum CE (~120.8 cd A^{-1}), whereas tandem OLEDs with the 4LG anodes showed CEs that decreased by only 6.6% (PET) and 11.7% (glass) (~193.2 cd A^{-1} (PET) and 181.7 cd A^{-1} (glass)) at ~10 000 cd m^{-2} compared with their maximum CEs. Because tandem OLEDs require much less current density than single-unit OLEDs to emit a same luminance, the populations of excitons and charge carriers are effectively reduced in organic layers; types of non-radiative exciton recombination such as triplet–polaron and triplet–triplet exciton annihilation can thus be minimized in tandem OLEDs. Therefore, tandem OLEDs with a low current density showed lower efficiency roll-off characteristics than single-unit OLEDs with 4LG anodes. Additionally, a 4LG anode on a PET substrate with lower sheet resistance showed lower device efficiency roll-off (~6.6%) than that on a glass substrate (~11.7%) because the higher sheet resistance of the 4LG on a glass substrate can change charge balance in devices under high applied bias. The EL spectra normalized to the maximum peak

intensity (~520 nm) were similar for single and tandem OLEDs with 4LG anodes (Figure 4d); the small differences between these spectra can be attributed to a change in the recombination position in OLED structures.[47] We also calculated EQEs of tandem OLEDs by analyzing the angular EL distribution according to viewing angles (Figure 4e). The tandem OLEDs with 4LG anodes exhibited very high maximum EQEs of ~45.2% with a PET substrate and ~44.4% with a glass substrate. We further improved the CEs, EQEs and efficiency roll-off characteristics by placing a hemispherical lens on the emitting surface of the tandem OLEDs with the 4LG anodes. By placing a hemispherical lens on the devices to enhance light out-coupling, we successfully achieved extremely efficient tandem OLEDs with the 4LG anodes that have significantly improved luminescent characteristics (CE: ~395.0 cd A^{-1} (PET) and ~396.4 cd A^{-1} (Glass); EQE: ~86.5% (PET) and ~87.3% (Glass)) (Figures 4b, f, and Supplementary Figure S5; Table 1 and Supplementary Table S4). Furthermore, the tandem OLEDs with the 4LG anodes and the hemispherical lens showed very low efficiency roll-off: the EQE was decreased by only 3.8% of the maximum (~83.4%) at luminance of ~10 000 cd m^{-2} with a PET substrates.

Various applications of flexible electronics require a guaranteed mechanical robustness of the flexible OLEDs. To demonstrate the mechanical flexibility of tandem OLEDs with the 4LG anode, we performed bending stability tests using the 4LG anode on a 200-μm-thick PET substrate. A repetition of the bending tests with ~1.33% strain (bending radius of curvature ~7.5 mm) rapidly dropped the current density of OLEDs with ITO anodes because the brittle ITO anode can crack easily when bending is applied with >1% strain.[48] A repetition of 500 bending cycles completely insulated OLEDs that have an ITO anode. In contrast, tandem OLEDs with the 4LG anode did not show significant changes in the current density upon 1000 bending cycles (Figure 5a). We also conducted a flexibility test according to bending strain by gradually reducing the bending radius of devices with ITO or 4LG anode. The current densities of devices were measured during flexion (Figure 5b inset). Increasing the bending strain drastically decreased the current density of OLEDs with an ITO anode and a bending strain of ~5% caused them to fail completely. Tandem OLEDs with 4LG anodes maintained nearly the same current density for a bending strain of up to ~6.7% that corresponds to a 1.5 mm bending radius of curvature (Figure 5b); a rollable display, which represents the ultimate form of flexible displays, requires a 5–10 mm bending radius of curvature, which is easily achievable in our flexible OLEDs.[49] This result demonstrates the excellent mechanical flexibility of tandem OLEDs with the 4LG anode relative to the external bending stress. In addition, we used the thin PET substrate (thickness: ~50 μm) to observe the excellent flexibility of tandem OLEDs with the 4LG anode. Figure 5c shows optical images of light emission from flexible tandem OLEDs with a graphene anode when wrapped around a cylindrical pencil (bending radius: ~7.7 mm, bending strain: ~0.65%) and around a very thin glass pipette (bending radius: ~0.87 mm, bending strain ~2.86%) (Figure 5c).

CONCLUSION

We fabricated flexible tandem OLEDs that had a very high CE (~205.9 cd A^{-1}), a high EQE (~45.2%) and a low efficiency roll-off (~6.6% CE decrease to emit 10 000 cd m^{-2}) by stacking two EL units vertically on a modified multi-layered graphene anode with a flexible PET substrate. The introduction of a hemispherical lens on the tandem OLEDs with a 4LG anode further improved their CEs to 396.4 cd A^{-1} and their EQEs to 87.3%. Furthermore, the device efficiency of tandem OLEDs with enhanced light out-coupling was nearly unchanged to emit a high luminance of ~10 000 cd m^{-2}. The modification strategy of the pristine 4LG anode to reduce its sheet resistance (~58.3 Ω per square) and increase its surface WF (>6.0 eV) facilitated hole injection from the graphene anode to the lower EL unit. An easily controllable and low-temperature evaporable Li_3N was employed as an n-type dopant in the CGL to effectively stack the upper EL unit on the lower one without causing damage to the OLEDs on thin flexible plastic substrates. Because this CGL efficiently generated and injected charges into adjacent HTL and ETL, the tandem OLEDs with the graphene anode exhibited remarkable device efficiencies and negligible efficiency roll-off by reducing the current density to emit a same luminance compared with that of single-unit OLEDs. Furthermore, flexible tandem OLEDs with plastic substrates exhibited excellent mechanical stability after bending tests of up to 1000 cycles and 6.7% strain. This approach to creating ultimate flexible tandem OLEDs with a very high device efficiency, a very low efficiency roll-off at a high luminance, and excellent flexibility will provide a significant step towards next-generation flexible displays and solid-state lighting with graphene anodes.

CONFLICT OF INTEREST

The authors declare no conflict of interest.

ACKNOWLEDGEMENTS

This work was supported by a National Research Foundation of Korea (NRF) grant funded by the by the Ministry of Science, ICT & Future Planning (MSIP) (NRF-2016R1A3B1908431), and the Nano Material Technology Development Program through the National Research Foundation of Korea (NRF) funded by the Ministry of Science, ICT & Future Planning (MSIP) (NRF-2014M3A7B4051747).

1 Kido, J., Kimura, M. & Nagai, K. Multilayer white light-emitting organic electroluminescent device. *Science* **267**, 1332–1334 (1995).
2 Friend, R. H., Gymer, R. W., Holmes, A. B., Burroughes, J. H., Marks, R. N., Taliani, C., Bradley, D. D. C., Dos Santos, D. A., Brédas, J. L., Lögdlund, M. & Salaneck, W. R. Electroluminescence in conjugated polymers. *Nature* **397**, 121–128 (1999).
3 Reineke, S., Lindner, F., Schwartz, G., Seidler, N., Walzer, K., Lussem, B. & Leo, K. White organic light-emitting diodes with fluorescent tube efficiency. *Nature* **459**, 234–238 (2009).
4 Helander, M. G., Wang, Z. B., Qiu, J., Greiner, M. T., Puzzo, D. P., Liu, Z. W. & Lu, Z. H. Chlorinated indium tin oxide electrodes with high work function for organic device compatibility. *Science* **332**, 944–947 (2011).
5 Wang, Z. B., Helander, M. G., Qiu, J., Puzzo, D. P., Greiner, M. T., Hudson, Z. M., Wang, S., Liu, Z. W. & Lu, Z. H. Unlocking the full potential of organic light-emitting diodes on flexible plastic. *Nat. Photon* **5**, 753–757 (2011).
6 Han, T.-H., Lee, Y., Choi, M.-R., Woo, S.-H., Bae, S.-H., Hong, B. H., Ahn, J.-H. & Lee, T.-W. Extremely efficient flexible organic light-emitting diodes with modified graphene anode. *Nat. Photon* **6**, 105–110 (2012).
7 Uoyama, H., Goushi, K., Shizu, K., Nomura, H. & Adachi, C. Highly efficient organic light-emitting diodes from delayed fluorescence. *Nature* **492**, 234–238 (2012).
8 White, M. S., Kaltenbrunner, M., Głowacki, E. D., Gutnichenko, K., Kettlgruber, G., Graz, I., Aazou, S., Ulbricht, C., Egbe, D. A. M., Miron, M. C., Major, Z., Scharber, M. C., Sekitani, T., Someya, T., Bauer, S. & Sariciftci, N. S. Ultrathin, highly flexible and stretchable PLEDs. *Nat. Photon* **7**, 811–816 (2013).
9 Kumar, A. & Zhou, C. The race to replace tin-doped indium oxide: which material will win? *ACS Nano* **4**, 11–14 (2010).
10 Cai, M., Ye, Z., Xiao, T., Liu, R., Chen, Y., Mayer, R. W., Biswas, R., Ho, K.-M., Shinar, R. & Shinar, J. Extremely efficient indium-tin-oxide-free green phosphorescent organic light-emitting diodes. *Adv. Mater.* **24**, 4337–4342 (2012).
11 Ou, E. C.-W., Hu, L., Raymond, G. C. R., Soo, O. K., Pan, J., Zheng, Z., Park, Y., Hecht, D., Irvin, G., Drzaic, P. & Gruner, G. Surface-modified nanotube anodes for high performance organic light-emitting diode. *ACS Nano* **3**, 2258–2264 (2009).
12 Yu, Z., Zhang, Q., Li, L., Chen, Q., Niu, X., Liu, J. & Pei, Q. Highly flexible silver nanowire electrodes for shape-memory polymer light-emitting diodes. *Adv. Mater.* **23**, 664–668 (2011).
13 Novoselov, K. S., Geim, A. K., Morozov, S. V., Jiang, D., Zhang, Y., Dubonos, S. V., Grigorieva, I. V. & Firsov, A. A. Electric field effect in atomically thin carbon films. *Science* **306**, 666–669 (2014).

14 Zhang, Y., Tan, Y., Stormer, H. L. & Kim, P. Experimental observation of the quantum Hall effect and Berry's phase in graphene. *Nature* **438**, 201–204 (2005).
15 Duong, D. L., Han, G. H., Lee, S. M., Gunes, F., Kim, E. S., Kim, S. T., Kim, H., Ta, Q. H., So, K. P., Yoon, S. J., Chae, S. J., Jo, Y. W., Park, M. H., Chae, S. H., Lim, S. C., Choi, J. Y. & Lee, Y. H. Probing graphene grain boundaries with optical microscopy. *Nature* **490**, 235–239 (2012).
16 Rogers, J. A. Electronic materials: making graphene for macroelectronics. *Nature Nanotech* **3**, 254–255 (2008).
17 Bonaccorso, F., Sun, Z., Hasan, T. & Ferrari, A. C. Graphene photonics and optoelectronics. *Nat. Photon* **4**, 611–622 (2010).
18 Kim, K. S., Zhao, Y., Jang, H., Lee, S. Y., Kim, J. M., Kim, K. S., Ahn, J.-H., Kim, P., Choi, J.-Y. & Hong, B. H. Large-scale pattern growth of graphene films for stretchable transparent electrodes. *Nature* **457**, 706–710 (2009).
19 Bae, S., Kim, H., Lee, Y., Xu, X., Park, J.-S., Zheng, Y., Balakrishnan, J., Lei, T., Kim, H. R., Song, Y. I., Kim, Y.-J., Kim, K. S., Özyilmaz, B., Ahn, J.-H., Hong, B. H. & Iijima, S. Roll-to-roll production of 30-inch graphene films for transparent electrodes. *Nat. Nanotech* **5**, 574–578 (2010).
20 Han, T.-H., Jeong, S.-H., Lee, Y., Seo, H.-K., Kwon, S.-J., Park, M.-H. & Lee, T.-W. Flexible transparent electrodes for organic light-emitting diodes. *J. Inf. Disp* **16**, 71–84 (2015).
21 Park, M.-H., Han, T.-H., Kim, Y.-H., Jeong, S.-H., Lee, Y., Seo, H.-K., Cho, H. & Lee, T.-W. Flexible organic light-emitting diodes for solid-state lighting. *J. Photon. Energy* **5**, 053599 (2015).
22 Wu, J., Agrawal, M., Becerril, H. A., Bao, Z., Liu, Z., Chen, Y. & Peumans, P. Organic light-emitting diodes on solution-processed graphene transparent electrodes. *ACS Nano* **4**, 43–48 (2010).
23 Sun, T., Wang, Z. L., Shi, Z. J., Ran, G. Z., Xu, W. J., Wang, Z. Y., Li, Y. Z., Dai, L. & Qin, G. G. Multilayered graphene used as anode of organic light emitting devices. *Appl. Phys. Lett.* **96**, 133301 (2010).
24 Han, T.-H., Kwon, S.-J., Li, N., Seo, H.-K., Xu, W., Kim, K.-S. & Lee, T.-W. Versatile p-Type Chemical Doping to Achieve Ideal Flexible Graphene Electrodes. *Angew. Chem. Int. Ed.* **55**, 6197–6201 (2016).
25 Li, N., Oida, S., Tulevski, G. S., Han, S.-J., Hannon, J. B., Sadana, D. K. & Chen, T.-C. Efficient and bright organic light-emitting diodes on single-layer graphene electrodes. *Nat. Comm* **4**, 2294 (2013).
26 Kim, D., Lee, D., Lee, Y. & Jeon, D. Y. Work-function engineering of graphene anode by bis(trifluoromethanesulfonyl)amide doping for efficient polymer light-emitting diodes. *Adv. Funct. Mater.* **23**, 5049–5055 (2013).
27 Meyer, J., Kidambi, P. R., Bayer, B. C., Weijtens, C., Kuhn, A., Centeno, A., Pesquera, A., Zurutuza, A., Robertson, J. & Hofmann, S. Metal oxide induced charge transfer doping and band alignment of graphene electrodes for efficient organic light emitting diodes. *Sci. Rep* **4**, 5380 (2014).
28 Kim, H., Bae, S.-H., Han, T.-H., Lim, K.-G., Ahn, J.-H. & Lee, T.-W. Organic solar cells using CVD-grown graphene electrodes. *Nanotechnology* **25**, 014012 (2014).
29 Chang, H., Wang, G., Yang, A., Tao, X., Liu, X., Shen, Y. & Zheng, Z. A transparent, flexible, low-temperature, and solution-processible graphene composite electrode. *Adv. Funct. Mater.* **20**, 2893–2902 (2010).
30 Hwang, J. O., Park, J. S., Choi, D. S., Kim, J. Y., Lee, S. H., Lee, K. E., Kim, Y.-H., Song, M. H., Yoo, S. & Kim, S. O. Workfunction-tunable, N-doped reduced graphene transparent electrodes for high-performance polymer light-emitting diodes. *ACS Nano* **6**, 159–167 (2012).
31 Lee, J., Han, T.-H., Park, M.-H., Jung, D. Y., Seo, J., Seo, H.-K., Cho, H., Kim, E., Chung, J., Choi, S.-Y., Kim, T.-S., Lee, T.-W. & Yoo, S. Synergetic electrode architecture for efficient graphene-based flexible organic light-emitting diodes. *Nat. Commun* **7**, 11791 (2016).
32 Cho, H., Kim, S. D., Han, T.-H., Song, I., Byun, J.-W., Kim, Y.-H., Kwon, S., Bae, S.-H., Choi, H. C., Ahn, J.-H. & Lee, T.-W. Improvement of work function and hole injection efficiency of graphene anode using CHF3 plasma treatment. *2D Mater* **2**, 014002 (2015).
33 Han, T.-H., Kwon, S.-J., Seo, H.-K. & Lee, T.-W. Controlled surface oxidation of multi-layered graphene anode to increase hole injection efficiency in organic electronic devices. *2D Mater* **3**, 014003 (2016).
34 Liao, L. S., SIusarek, W. K., Hatwar, T. K., Ricks, M. L. & Comfort, D. L. Tandem organic light-emitting diode using hexaazatriphenylene hexacarbonitrile in the intermediate connector. *Adv. Mater.* **20**, 324–329 (2008).
35 Lee, T.-W., Noh, T., Choi, B.-K., Kim, M.-S., Shin, D. W. & Kido, J. High-efficiency stacked white organic light-emitting diodes. *Appl. Phys. Lett.* **92**, 043301 (2008).
36 Shin, W. C., Yoon, T., Mun, J. H., Kim, T. Y., Choi, S.-Y., Kim, T.-S. & Cho, B. J. Doping suppression and mobility enhancement of graphene transistors fabricated using an adhesion promoting dry transfer process. *Appl. Phys. Lett.* **103**, 243504 (2013).
37 Mattevi, C., Kim, H. & Chhowalla, M. A review of chemical vapour deposition of graphene on copper. *J. Mater. Chem.* **21**, 3324–3334 (2011).
38 Das, A., Pisana, S., Chakraborty, B., Piscanec, S., Saha, S. K., Waghmare, U. V., Novoselov, K. S., Krishnamurthy, H. R., Geim, A. K., Ferrari, A. C. & Sood, A. K. Monitoring dopants by Raman scattering in an electrochemically top-gated graphene transistor. *Nat. Nanotech* **3**, 210–215 (2008).
39 Casiraghi, C. Doping dependence of the raman peaks intensity of graphene close to the dirac point. *Phys. Rev. B* **80**, 233407 (2009).
40 Lin, L.-B., Young, R. H., Mason, M. G., Jenekhe, S. A. & Borsenberger, P. M. Transient photocurrents across organic–organic interfaces. *Appl. Phys. Lett.* **72**, 864 (1998).
41 Kim, S.-Y., Jeong, W.-I., Mayr, C., Park, Y.-S., Kim, K.-H., Lee, J.-H., Moon, C.-K., Brütting, W. & Kim, J.-J. Organic light-emitting diodes with 30% external quantum efficiency based on a horizontally oriented emitter. *Adv. Funct. Mater.* **23**, 3896–3900 (2013).
42 Zardetto, V., Brown, T. M., Reale, A. & Carlo, A. D. Substrates for flexible electronics: a practical investigation on the electrical, film flexibility, optical, temperature, and solvent resistance properties. *J. Polym. Sci., Part B: Polym. Phys* **49**, 638–648 (2011).
43 Choi, M.-C., Kim, Y. & Ha, C.-C. Polymers for flexible displays: from material selection to device applications. *Prog. Polym. Sci.* **33**, 581–630 (2008).
44 Duan, L., Liu, Q., Li, Y., Gao, Y., Zhang, G., Zhang, D., Wang, L. & Qiu, Y. Thermally decomposable lithium nitride as an electron injection materials for highly efficient and stable OLEDs. *J. Phys. Chem. C* **113**, 13386–13390 (2009).
45 Yang, J.-P., Xiao, Y., Deng, Y.-H., Duhm, S., Ueno, N., Lee, S.-T., Li, Y.-Q. & Tang, J.-X. Electric-field-assisted charge generation and separation process in transition metal oxide-based interconnectors for tandem organic light-emitting diodes. *Adv. Funct. Mater.* **22**, 600–608 (2012).
46 Bao, Q. Y., Yang, J. P., Li, Y. Q. & Tang, J. X. Electronic structures of MoO_3-based charge generation layer for tandem organic light-emitting diodes. *Appl. Phys. Lett.* **97**, 063303 (2010).
47 Kahen, K. B. Rigorous optical modeling of multilayer organic light-emitting diode devices. *Appl. Phys. Lett.* **78**, 1649 (2001).
48 Lee, M.-S., Lee, K., Kim, S.-Y., Lee, H., Park, J., Choi, K.-H., Kim, H.-K., Kim, D.-G., Lee, D.-Y., Nam, S. W. & Park, J.-U. High-performance, transparent, and stretchable electrodes using graphene-metal nanowire hybrid structures. *Nano Lett.* **13**, 2814–2821 (2013).
49 Park, S.-I., Ahn, J.-H., Feng, X., Wang, S., Huang, Y. & Rogers, J. A. Theoretical and experimental studies of bending of inorganic electronic materials on plastic substrates. *Adv. Funct. Mater.* **18**, 2673 (2008).

Supplementary Information accompanies the paper on the NPG Asia Materials website (http://www.nature.com/am)